Supplemental Figure 1

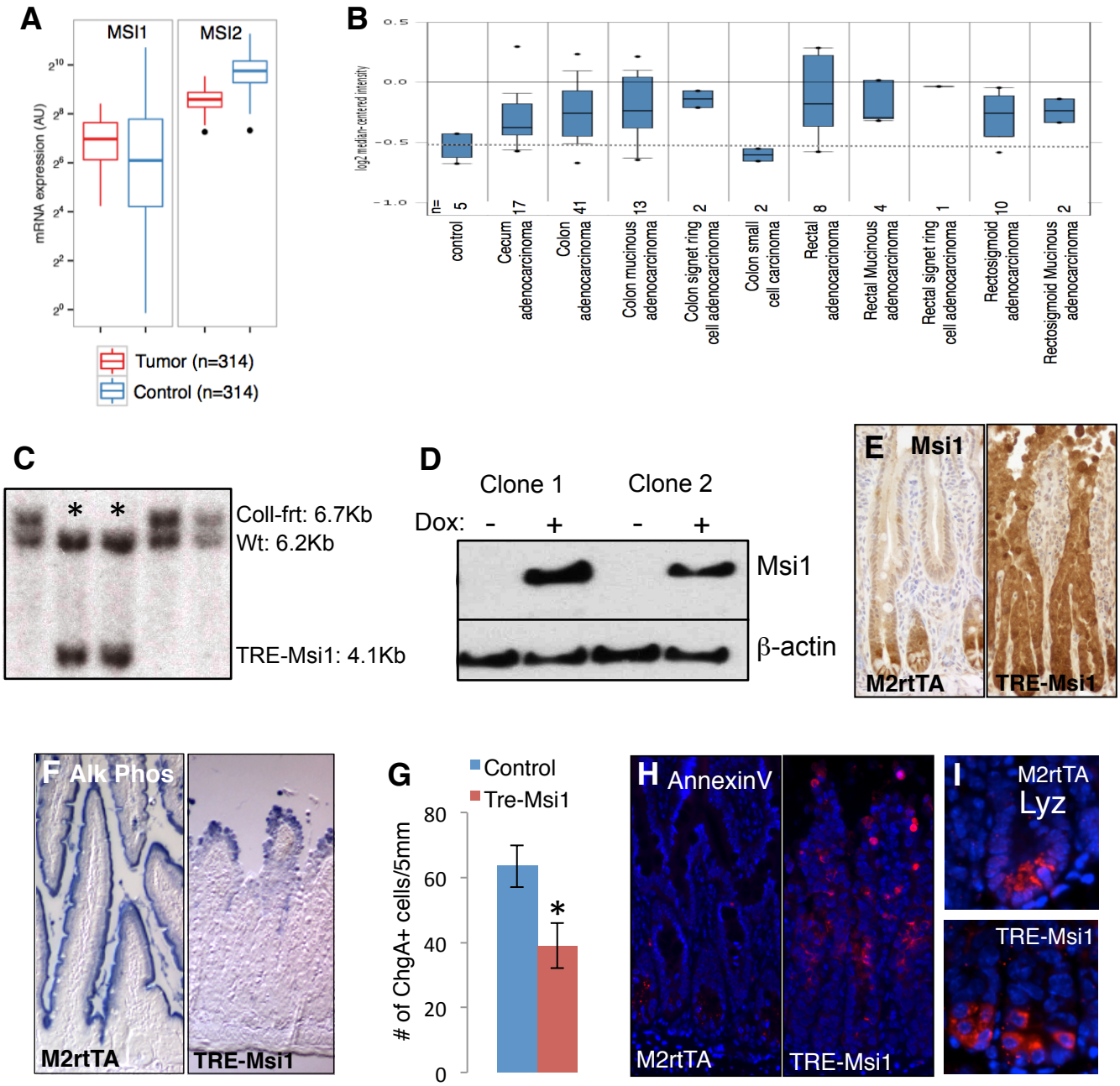

Supplemental Figure 1, related to Figure 1. A. TCGA data analysis comparing expression of MSI1 vs. MSI2 in a panel of 314 colorectal adenocarcinomas and 314 normal controls (non patient-matched). **B.** Oncomine transcriptome profiling data of *MSI1* expression in a panel of human gastrointestinal cancers relative to control tissue. The number of samples for each tumor type are indicated. **C.** Southern blot demonstrating correct flip-in targeting (asterisk) of the *TRE-Msi1* allele downstream of the *Coll1a1* locus. **D.** Dox-induction of the *TRE-Msi1* allele in targeted ES cell clones shown by immunoblot. **E.** Immunohistochemistry for Msi1 in control (*M2rtTA*+Dox) and *TRE-Msi1* intestinal epithelium 48hrs after Dox induction. **F.** Staining for Alkaline Phosphatase activity in enterocytes of control (*M2rtTA*+Dox) and *TRE-Msi1* intestinal epithelium. **G.** Quantification of Chromogranin-A-positive enteroendocrine cells per 5mm of small intestine (micrograph shown in Main Figure 1H). *: $p<0.05$, n=4 mice per group. **H.** Immunofluorescence staining for apoptotic cells with annexin-V. **I.** Immunofluorescence detecting Paneth cells at the crypt base via Lysozyme staining in control (*M2rtTA*) and *TRE-Msi1* mice treated with Dox for 48 hours (mag. 400x).

Supplemental Figure 2

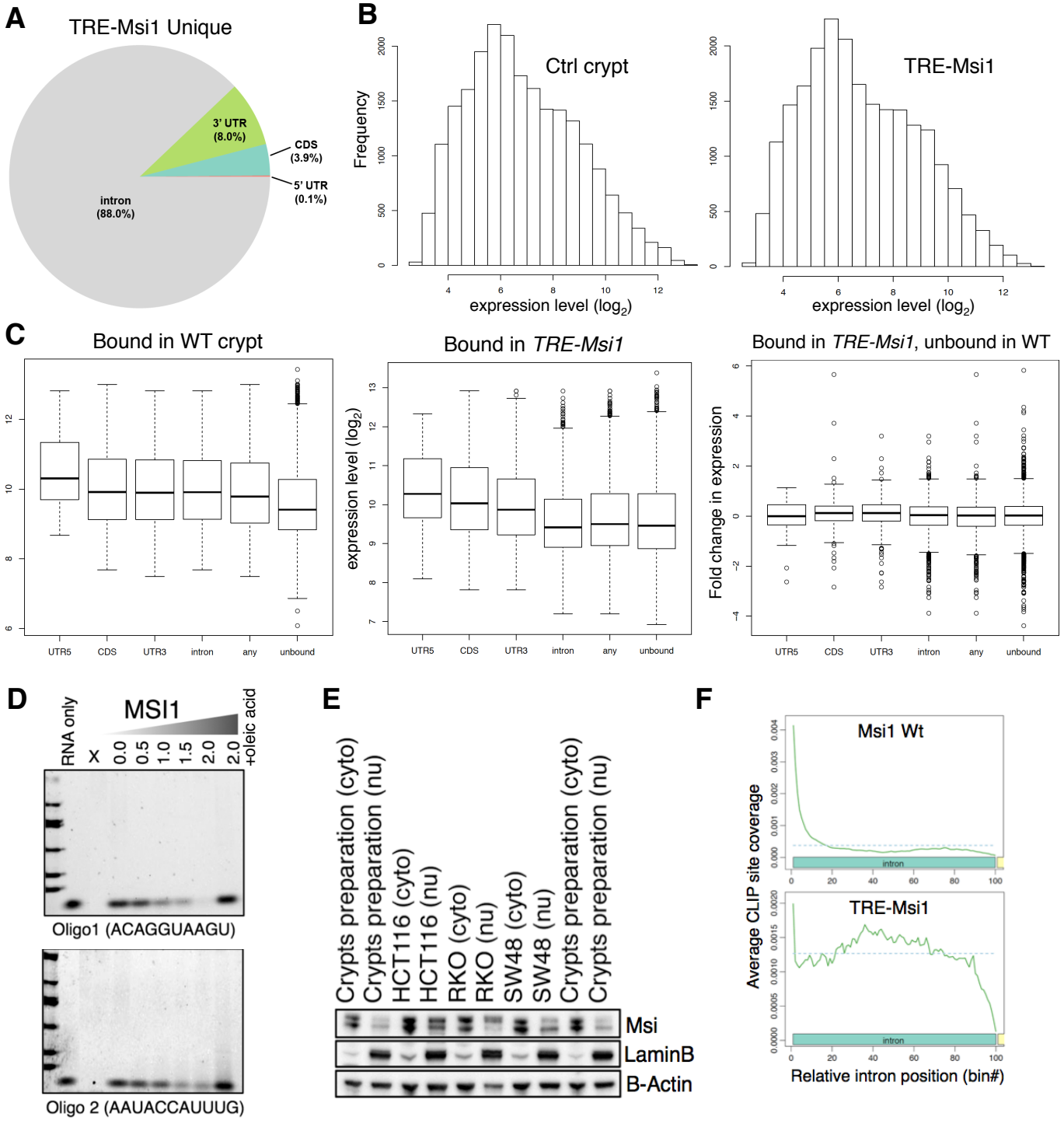

Supplemental Figure 2, related to Figure 3. A Distribution of Msi1 binding events occurring only in *TRE-Msi1* epithelium and not in wildtype crypts. **B.** Expression levels of Msi1 CLIP targets plotted against the frequency of binding events in wildtype crypts and *TRE-Msi1* epithelium. **C.** Expression levels of Msi1 CLIP targets of various classes, including the change in expression of genes newly bound after *TRE-Msi1* activation relative to wildtype crypts (right panel). **D.** Msi1 RNA binding assays demonstrating dose-dependent interaction between Msi1 and consensus motif oligos derived from CLIP studies (shown in **Figure 3d**). Msi1 binding is competed by the known allosteric Msi inhibitor oleic acid. **E.** Cytoplasmic-Nuclear (cyto/nu) fractionation of human colorectal cancer cell lines and primary wildtype intestinal crypts showing predominantly cytoplasmic Msi localization, with detectable nuclear localization particularly in cancer cells. **F.** Metaprofiles for Msi1 binding location across introns.

Supplemental Figure 3

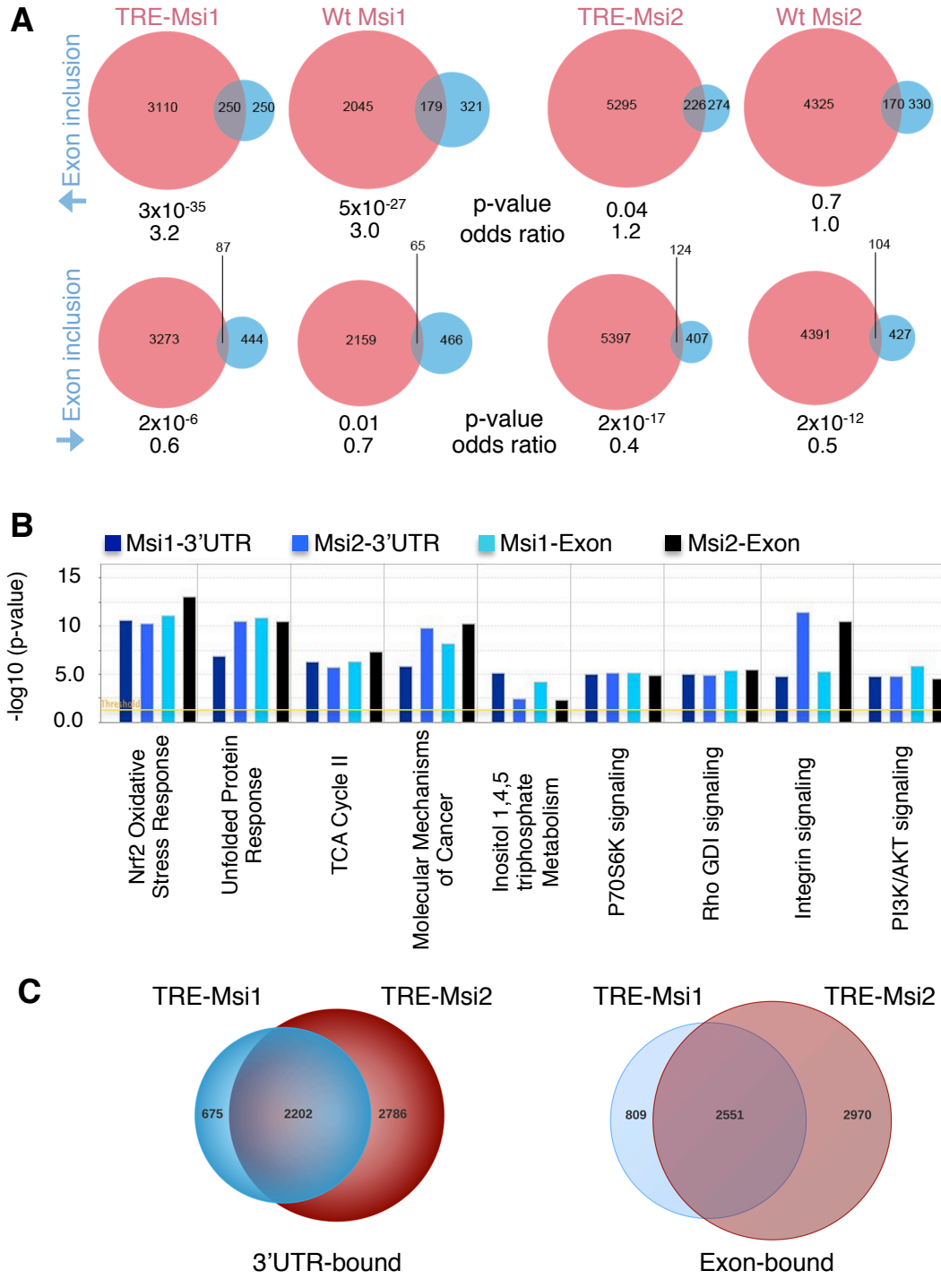

Supplemental Figure 3, related to Figure 3. A. Msi CLIP target overlap with transcripts exhibiting alternative splicing in upon Msi1 induction. Transcripts exhibiting increased exon inclusion (blue circles, top) or decreased exon inclusion (blue circles, bottom) in *TRE-Msi1* epithelium vs. control were overlapped with Msi CLIP targets (CLIP target sets indicated in red). **B.** Ingenuity Pathway Analysis (IPA) of canonical pathways represented in Msi CLIP target sets. p-values are derived using Fisher's exact test. **C.** Venn diagrams showing overlap between Msi1 and Msi2 RNA-binding targets in total epithelium from *TRE-Msi1* and *TRE-Msi2* mice.

Supplemental Figure 4

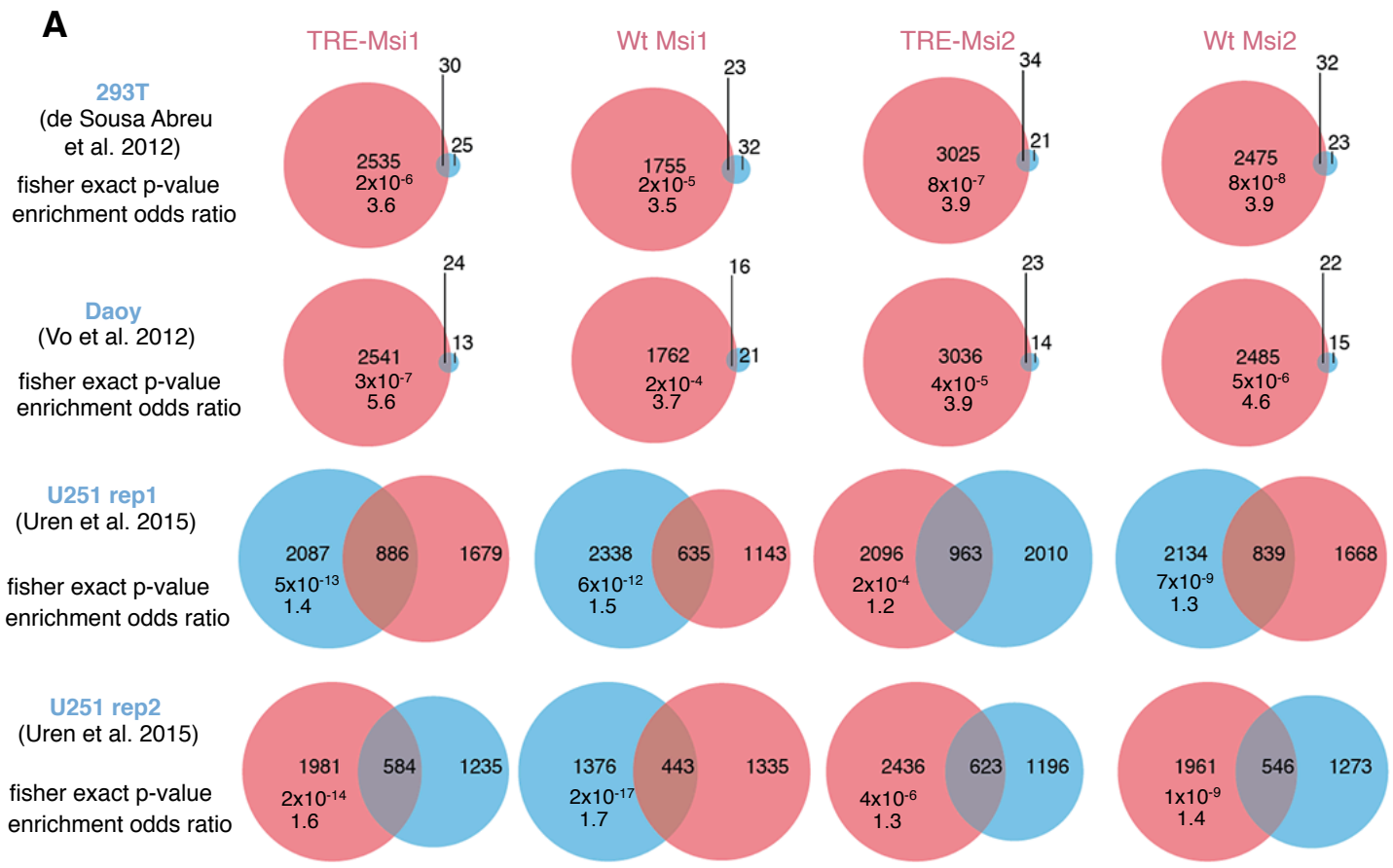

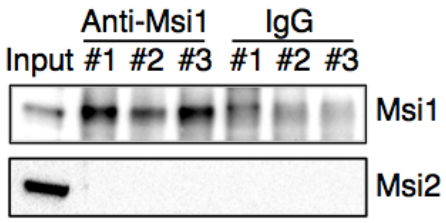

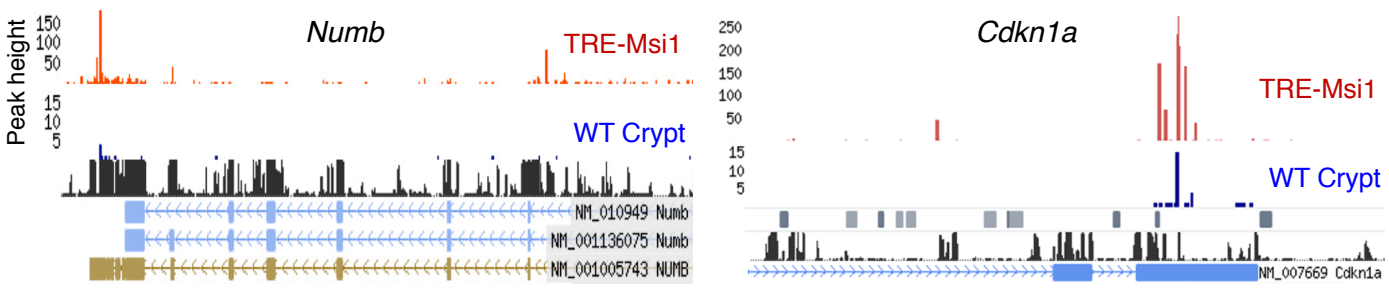

Supplemental Figure 4, related to Figure 3. A. Overlap between Msi1 or Msi2 CLIP targets identified in our *in vivo* dataset and MSI1 targets identified *in vitro* in transformed human cell lines (DAOY medulloblastoma, HEK293T embryonic kidney, and two replicates of U251 glioblastoma). **B.** Immunoprecipitation of Msi1 followed by Western blotting for Msi1 and Msi2 revealing no detectable protein-protein interaction **C.** CLIP-Seq tracks showing Msi1 binding to the transcripts encoding Numb (left) and p21 (Cdkn1a, right).

Supplemental Figure 5

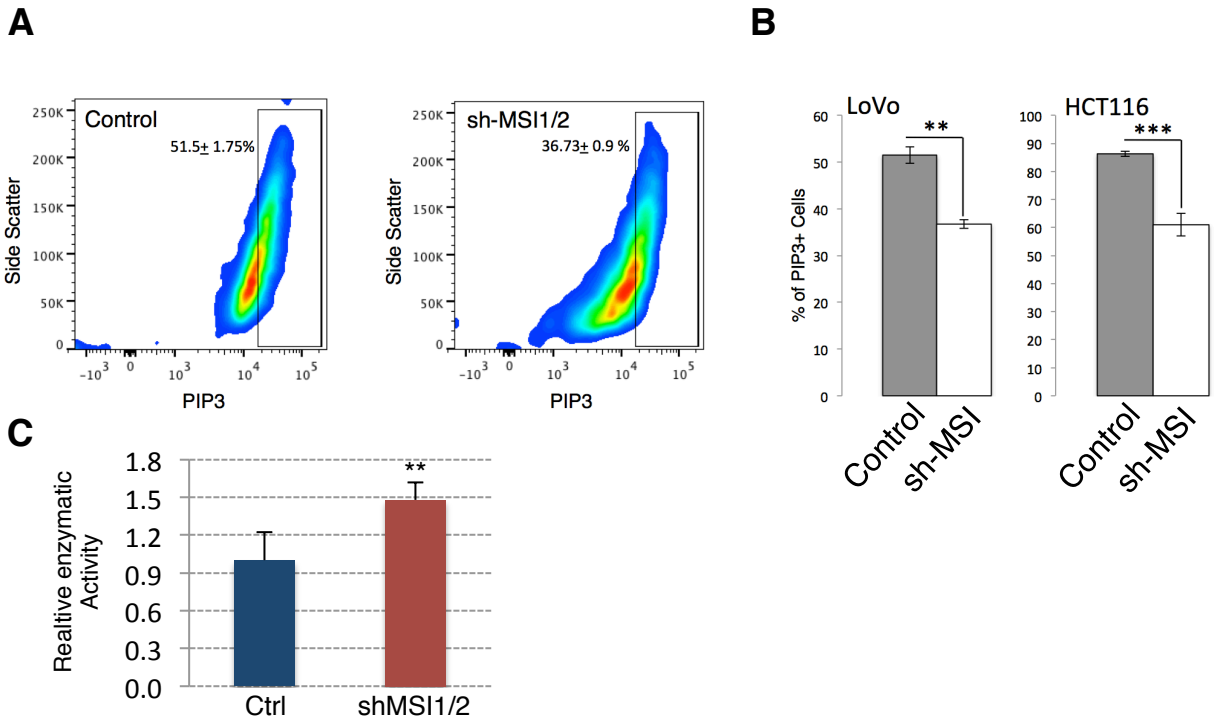

Supplemental Figure 5, related to Figure 5. A.. Flow cytometric analysis of PIP3 in LoVo cells upon knockdown of MSI1 and MSI2. **B**. Quantification of PIP3 flow cytometric analysis shown in (**A**) in LoVo and HCT116 cells upon MSI1/2 knockdown**. C.** PTEN enzymatic activity (measured by immunoprecipitation followed by ELISA) increases upon knockdown of MSI1/2 in RKO cells versus scrambled shRNA control. **: $p < 0.005$, ***: $p < 0.0005$, n=3, Student's t-test.

Supplemental Figure 6

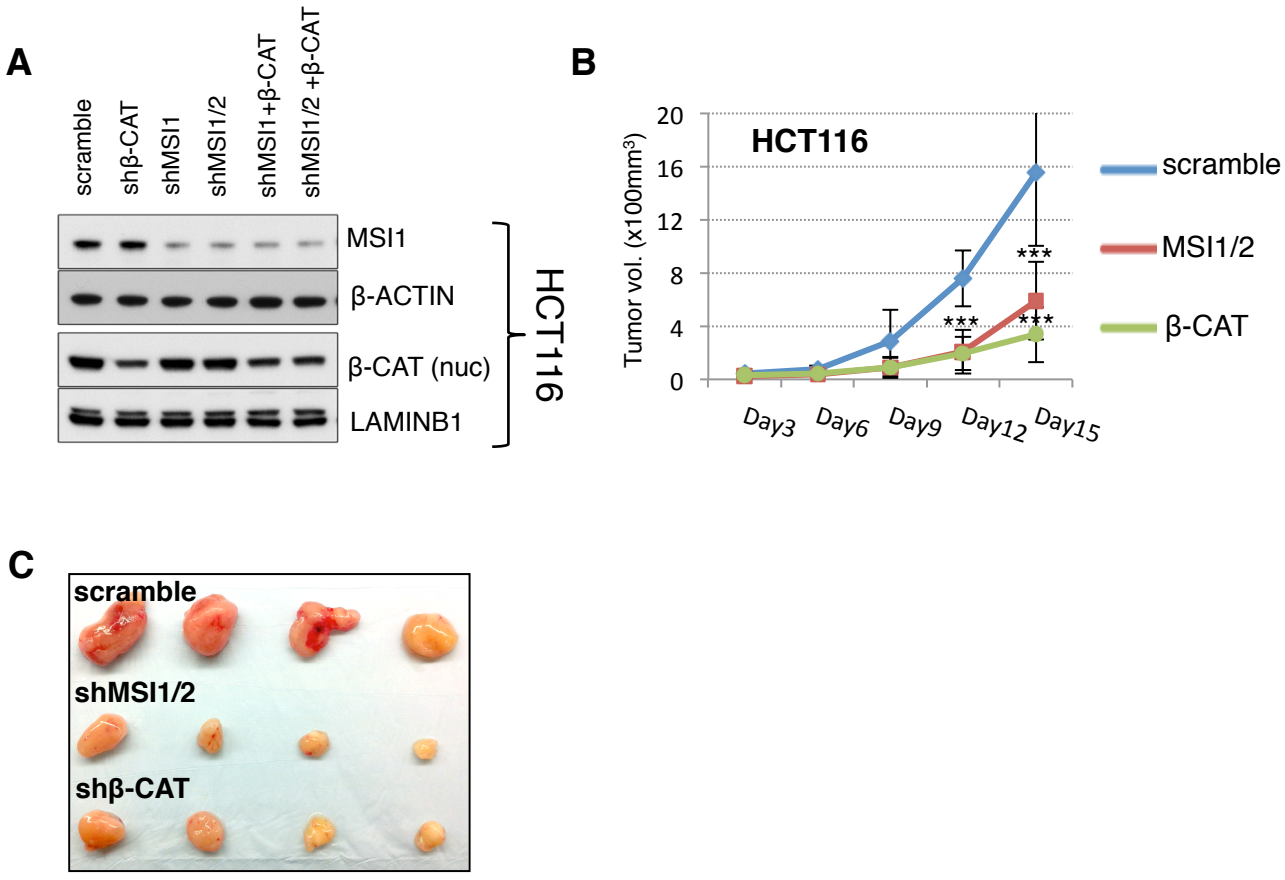

Supplemental Figure 6, related to Figure 6. A. Immunoblotting for MSI1 and nuclear B-CATENIN in HCT116 cells. **B-C.** Growth of HCT116 cell xenografts upon MSI or β-CATENIN shRNA knockdown (**B**), with tumors shown after dissection upon termination of the experiment (**C**). ***: p< 0.0005., Student's t-test.

Supplemental Figure 7

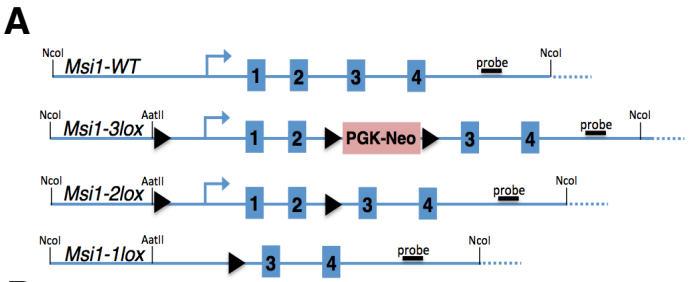

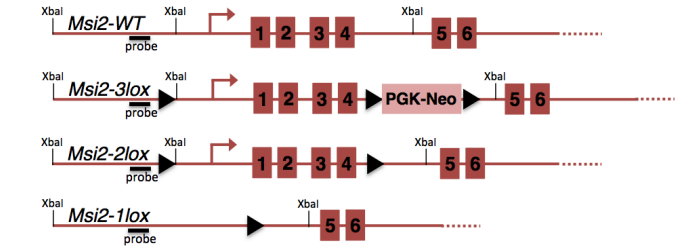

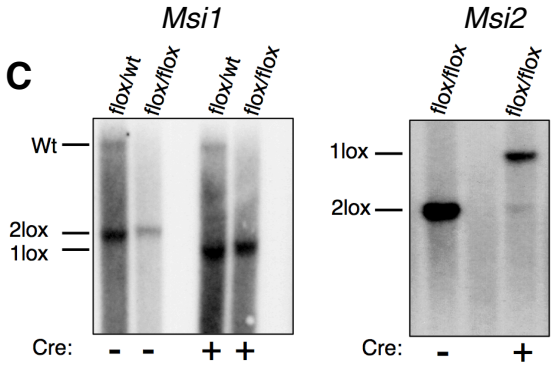

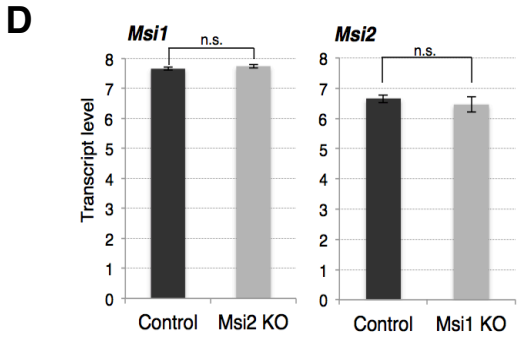

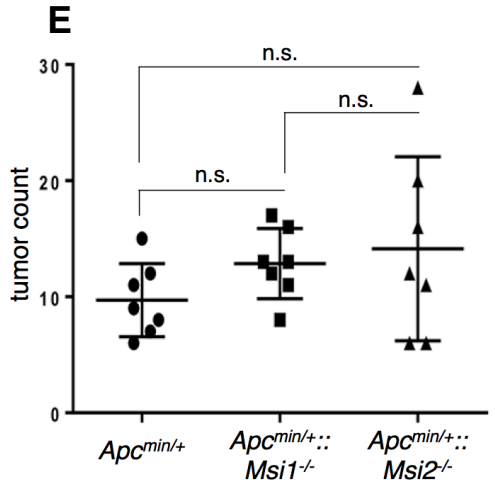

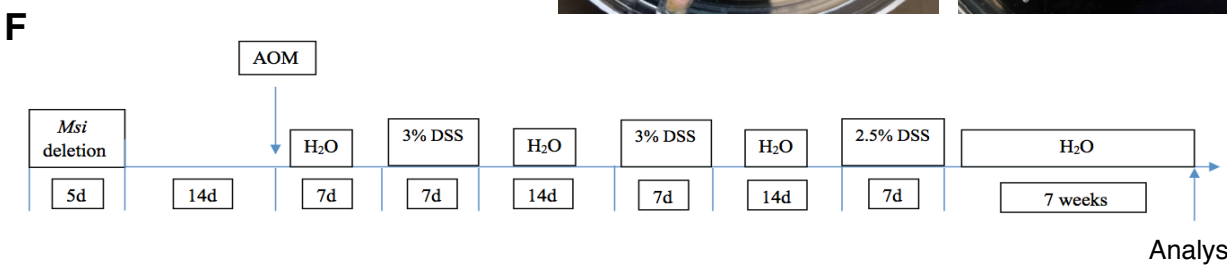

Supplemental Figure 7, related to Figure 7. A, B. Targeting strategy showing the *3-lox* alleles after homologous recombination in ES cells, the *2-lox (floxed)* alleles used to generate mouse strains after transient Cre introduction to excise the *PGK-Neo* cassette in culture, and the *1-lox*, null allele generated after Cre recombinase activity from the *Villin-CreER* transgene *in vivo*. **C.** Validation of *Villin-CreER* deletion of *Msi1* and *Msi2* by Southern blotting after digestion of genomic DNA with XbaI using an external 5' probe depicted in **A, B.** **D.** Expression levels of *Msi1* in *Msi2KO* mice one week after *Villin-CreER* deletion, and of *Msi2* in *Msi1KO* mice. **E.** Intestinal adenoma counts from $APC^{min/+}$ mice, $APC^{min/+::}Msi1^{-/-}$ mice, and $APC^{min/+::}Msi2^{-/-}$ mice after deletion of *Msi* genes using *Villin-CreER,* n=6-7 mice per group. **F.** Schematic of AOM-DSS protocol. *Msi1/2* deletion is mediated by *Villin-CreER* **G.** Photograph of colons resected from control (left) and *Msi1/2* double knockout (right) mice at the end of the AOM-DSS protocol.

Supplemental Tables

Supplemental Table 1, related to Figure 2: TRE-Msi1 transcriptome profiling. Expression profiling data for Dox-inducible Msi1 expression in primary small intestinal epithelium 24 hours after Dox induction versus control epithelium.

Supplemental Table 2, related to Figure 2: Gene Set Enrichment Analyses for TRE-Msi1 transcriptome changes. GSEA results derived from querying the TRE-Msi1 vs. Control transcriptome profiles from Supplemental Table 1 against the C2 curated all database.

Supplemental Table 3, related to Figure 3: Gene Ontology Analyses for Msi1 vs. Msi2-induced transcriptome changes. DAVID GO analysis of transcriptome changes common to both TRE-Msi1 and TRE-Msi2 versus control, as well as those unique to Tre-Msi1 or Tre-Msi2.

Supplemental Table 4, related to Figure 3: Msi1 RNA binding targets. *In vivo* RNA binding targets of Msi1 identified by crosslinking, immunoprecipitation, and massively parallel sequencing (CLIP-Seq), including endogenous Msi1 (small intestinal crypts) and ectopic Msi1 24 hours after Dox induction in the intestinal epithelium.

Supplemental Table 5, related to Figure 3: Gene Ontology Analyses for Msi1 vs. Msi2 *in vivo* RNA binding targets. GO analysis including endogenous Msi1/2 (small intestinal crypts) and ectopic Msi1/2 24 hours after Dox induction in the intestinal epithelium. Also included is the analogous analysis for an unrelated RNA binding protein, Lin28b.

Supplemental Table 6, related to Figure 3: Ingenuity Pathway Analysis (IPA) for Msi1/2 RNA binding targets. IPA analysis for pathways enriched in the Msi1 and Msi2-bound transcript list, bound either in their 3'UTRs or in exonic regions.

Supplemental Methods

Doxycycline Induction and Isolation of Intestinal Epithelium

For Dox induction of control (*M2rtTA* alone), and *TRE-Msi1* mice, 0.2-2mg/mL of Dox (Doxycycline hyclate, Sigma) was added to the drinking water along with 1% w/v sucrose of mice 2-3 months of age. All analysis of Dox-induced epithelium was performed 48 hours after induction, unless stated otherwise (24 hours used for CLIP and transcriptome profiling). For isolation of intestinal epithelial cells, mouse intestine was cut longitudinally and washed 2-3 times with ice-cold PBS, then cut into small pieces (1 cm long) and incubated for 1 hour at 4 °C in PBS containing 2 mM EDTA and 0.2 mM DTT on a rotating platform. Intestinal epithelial

cells were released by vortexing. For isolation of intestinal crypts, mouse small intestine was isolated and rinsed in PBS as above. The villi were scraped using a hemocytometer coverslip. The crypts were released from murine small intestine by incubation for 30 min at 4 °C in PBS containing 2 mM EDTA. Isolated crypts were counted and pelleted as described in (Sato et al., 2009).

Administration of Rapamycin

Rapamycin (LC Laboratories) was administered by daily intraperitoneal injection (4 mg per kg of body weight) for 5 days. It was reconstituted in absolute ethanol at 10 mg/ml and diluted in 5% Tween-80 (Sigma) and 5% PEG-400 (Hampton Research) before injection. The final volume of all injections was 200 ul. Dox was administered to *TRE-Msi1* mice for 48hours after the third dose of Rapamycin prior to euthanasia.

Histology, Immunofluorescence, and Immunochemistry

Intestines were washed with PBS, fixed in 10% Formalin, paraffin-embedded and sectioned. Hematoxylin, eosin, Alcian blue, and Alkaline Phosphatase staining was performed in the Morphology Core of the Penn Center for Molecular Studies in Digestive and Liver Diseases. For immunohistochemistry staining, antigen-retrieval was performed by heating slides in 0.01 M citrate buffer (pH 6) with a pressure cooker. The sections were then immunostained by the ABC peroxidase method (Vector labs) with diaminobenzidine (DAB) as the enzyme substrate and hematoxylin as a counterstain. For detection of nuclear β-catenin, antibody clone 15B8 (Sigma; 1:1000) was used in combination with the MOM kit (Vector Laboratories). For immunofluorescence staining, paraffin sections were pretreated in 0.01 M citrate buffer (pH 6) with a pressure cooker, and incubated in primary antibodies, then incubated with Cy2- or Cy3- conjugated fluorescent secondary antibodies (Jackson Laboratory) and counterstained with DAPI in mounting media (Vector labs). The following antibodies were used: Ki67 (Leica), Msi1 (MBL), Lysozyme (Santa Cruz), Chromogramin A (Abcam), GFP (Abcam). Crypt numbers per 1 mm were counted based on 25 randomly selected areas (Figure 1i). Crypt numbers per 1 mm were counted based on 20 randomly selected areas in proximal and distal intestine (Figure 5F), crypt height was measured based on 40 crypts (Figure 5G) (n=3 independent pairs of mice).

CLIP-Seq and CLIP-qRT-PCR

CLIP-Seq libraries were made as previously described in (Chi et al., 2009) with modifications. Total intestinal epithelial cells from two individual *TRE-Msi1* mice treated with Dox for 24 hours were isolated as above, and wildtype intestinal crypts from two control mice were isolated as above. For crosslinking, cell suspension was exposed to 2 pulses of 265nm UV light at 400mJ/cm^2 in a Stratalinker (Model 2400, Stratagene). Epithelial cells were then lysed using PXL buffer (PBS, 01% SDS, 0.5% deoxycholate, 0.5% NP-40, plus protease inhibitor and RNAsin). The lysates were sequentially treated with DNaseI and RNase, and spun in ultra-microcentrifuge at 40,000g for 20 min. The supernatant was added to protein A Dynabeads (Dynal, 100.02) conjugated with Msi1 antibody (AB5977, Millipore) and incubated for 4 hours at 4 °C. ^{32}P-γ-ATP labeled 3' RNA (RL-3) linker was ligated to the RNA fragment on beads overnight at 16°C. The beads were re-suspended in 30 μl of Novex loading buffer (without reducing agent), and separated with Novex NuPAGE 10% Bis-Tris gel and transferred to S&S BA-85 nitrocellulose membrane. After overnight exposure, around 50 KD band was visualized and the corresponding membrane was cut to small pieces. The RNA was released by proteinase K digestion and isolated using RNA phenol and $CHCl_3$ solution. 5' RNA (RL-5) linker was ligated into the RNA fragments. The RNA was transcribed into complementary DNA using RT-PCR and amplified using Re-PCR with Solexa fusion primers. The CLIP library underwent single-end sequencing on an Illumina hiSeq2000 at the University of Pennsylvania Functional Genomics Core. RL-3: 5'-OH GUG UCA GUC ACU UCC AGC GG 3' –puromycin; RL-5: 5' –OH AGG GAG GAC GAU GCG G 3'-OH. Adaptor sequences ('GTGTCAGTCACTTCCAGCG') were removed from the 3' end using the fastx-toolkit (http://hannonlab.cshl.edu/fastx_toolkit/). Reads were then mapped using Bowtie (-k 100 -n 0) to the mouse genome (mm9) (Langmead et al., 2009). Peaks were then called using an FDR ≤ 0.05 and motifs were identified using Homer (http://biowhat.ucsd.edu/homer/). The peaks were then annotated using a set of customized Perl and R scripts. CLIP-Seq datasets are available through GEO, accession number GSE54598.

For CLIP-qRTPCR, HEK 293 cells treated with GSK3β inhibitor or untreated control were crosslinked and immunoprecipitated with anti-MSI1 antibody as above. Immunoprecipitated

RNA was subjected to quantitative RT-PCR analysis after reverse transcription using a first strand synthesis kit (Invitrogen) and primers specific to the 3'UTRs of *APC* or *CTTNB1* in an ABI Prism quantitative PCR machine using standard 2 stage cycling protocols and SYBR green detection (n=3 biological replicates).

Gene Ontology Enrichment

Gene Ontology enrichment analyses of transcripts with Msi1 and Msi2 binding sites was performed using the DAVID online tool as previously described (Huang da et al., 2009). We define a background set of transcripts accessible to CLIP analysis as those with detectable expression in a tissue-matched RNA-Seq dataset (Middendorp et al., 2014). For this analysis, multiple isoforms of a single gene were only counted as one gene. To reduce bias in reporting GO terms, we report all GO terms within fourteen branches of the “biological process”, “molecular function”, and “cellular component” roots, as determined by a depth first search (Vandivier et al., 2013). Only terms enriched at FDR < 0.05 in at least two samples are reported.

Overlap with Published Human Msi1 CLIP and RIP Datasets

Only transcripts with homologues in both mice and humans were considered in this analysis. Human transcripts with RIP-Seq peaks (de Sousa Abreu et al., 2009; Vo et al., 2012) or CLIP-Seq peaks (Uren et al., 2015) were overlapped with mouse transcripts containing Msi1 and Msi2 CLIP-Seq peaks from our analysis. For significance testing, we define a “universe” of accessible transcripts as all mouse transcripts with 1) homology to human transcripts and 2) detectable expression in a tissue-matched RNA-Seq dataset (Middendorp et al., 2014). Significance of overlap was determined using a Fisher’s Exact test.

Overlap with Alternatively Spliced Transcripts

Exons with significantly (FDR < 0.05) higher or lower inclusion in Msi1 transgenic (TG) over wildtype (WT) were determined by microarray analysis, with three replicates of each genotype. All transcripts represented on the microarray exclusively show increased or decreased exon inclusion and not a combination of the two. Transcripts with differential exon inclusion were then overlapped with transcripts containing Msi1 and Msi2 CLIP-seq peaks in

our analysis. For significance testing, we define a "universe" of accessible genes as those 1) present on the microarray and 2) with detectable expression in a tissue-matched RNA-seq dataset (Middendorp et al., 2014). Significance of overlap was determined using a Fisher's Exact test.

Intron CLIP-Seq Peak Metaprofiles

CLIP-Seq peak coverage was computed at all mm9 RefSeq introns. Each intron was then length-normalized by binning to 100 intervals, and the average of bins across all introns is plotted as a meta-intron.

Transcriptome Profiling

Total RNA was isolated from total mouse small intestinal epithelial cells from 3 *M2rtTA* and 3 *TRE-Msi1* mice administered Dox for 24 hours in the drinking water using TRIzol Reagent (Life Technologies) according to the manufacturer's instructions. Total RNA was DNAse treated with an RNAse-free DNAse kit (Zymo Research). Purified RNA was submitted to the University of Pennsylvania Molecular Profiling Core, where samples were labeled and hybridized to Affymetrix Mouse Gene 1.0ST arrays. Microarray data was analyzed using Partek® Genomics Suite™ software. Following RMA background subtraction and normalization, a 1-way-ANOVA analysis between controls (*M2rtTA*) and Msi1 induced (*TRE-Msi1*) was run to compute *p-values* of significance and *F-statistic* for each probeset. *q-value*, a measure of false discovery rate (FDR) was computed within the SAM (Significance Analysis of Microarrays) software for each probeset by running an unpaired *t-test*. The FDR values were integrated with the 1-way-ANOVA results. Genes that were significant at FDR cut-off of 5% and changed at least 2-fold in either direction in the Msi1 induction group when compared to the control group were selected as the set of differentially expressed genes. This set of 836 unique genes and 6 samples were subjected to agglomerative hierarchical clustering analysis. Log2 intensities were median-centered across samples. Euclidean distance was used as the dissimilarity metric and average linkage method as clustering strategy. Results were visualized as intensity heatmap (Figure 2E). GEO accession numbers for microarray datasets are pending. Gene set enrichment analysis (GSEA) was run against the c2 curated gene sets of the Molecular Signatures Database (MSigDB) v3.0 comparing *M2rtTA* and *TRE-*

Msi1 groups to find statistically significant enriched gene sets.

For analysis of direct β-catenin target gene expression in Figure 4H, genes with published evidence for direct regulation by β-catenin demonstrated by chromatin immunoprecipitation were selected. These genes include *Edn1, Fra-1 (Fosl1), c-Myc, Met, c-Jun, Pinx1, Tcf4, Egfr, Klf5, Cyclin D (Ccnd1), Mycbp, Mmp7, Cdkn2a, Vegfa, SNAI1, Fgf18, Gja1 (connexin-43), Axin2, Claudin1, Runx2, Lef1, Bglap, ENPP2, Nrcam, DLK1, Vcan, Fgf4, Fn1, Tcf1, (Hnf1a), Lgr5, Ppard, Sp5, Ovol1, Id2, L1CAM, Cdh1 (E-cadherin), Fst, Tnfrsf19, Neurod1, Ctla4, Wisp1, Fzd7, Mitf, Pou3f2, Gbx2, Nkx2-2, Neurog1, Eda, T, Pitx2, Btrc, Cdx1, Birc5 (survivin), Pkd1, Pml, and Lect2 (chemotaxin2)*.

Reporter Assays

HCT116 cells were plated in 24-well-plate and transfected, in triplicate, with 0.5μg reporter vector (TOPflash Wnt reporter, FOPflash control reporter) together with 0.5μg of the human MSI1 expression vector (in pCDNA6) using FUGENE 6 transfection reagent (Promega). 48h after transfection cells were harvested for reporter assay using the Dual Luciferase Reporter Assay Kit (Promega) according to manufacturer's instruction. Reporter activity was measured using a Fluoroskan Ascent FL (Thermo).

Western Blots

Cells were lysed in RIPA buffer with protease inhibitors (Roche). After quantification using a BCA protein assay kit (Pierce), 20 μg of total protein was separated by 12% SDS-PAGE under denaturing conditions and transferred to PVDF membranes (GE Healthcare). Membranes were blocked in 5% BSA (Sigma) and then incubated with an anti-Msi1 primary antibody (1:1,000; Abcam), NICD (1:1,000; Abcam), Hes1 (1:1,000; Abcam), p-c-Raf (1:1,00; Cell Signaling), p-AKT (T308) (1:1,000; Cell Signaling), p-AKT (S473) (1:1,000; Cell Signaling), total-AKT (1:1,000; Cell Signaling), p-PDK1 (S241) (1:1,000; Cell Signaling), p-4EBP1 (T37/46) (1:1,000; Cell Signaling), or p-eIF4E (S209) (1:1,000; Cell Signaling), followed by incubation with a secondary antibody conjugated with horseradish peroxidase (HRP) (1:2,000; Cell Signaling) together with an HRP-conjugated primary antibody for β-actin

(1:10,000; Sigma). Immunoreactive proteins were visualized using LumiGLO chemiluminescent substrate (Pierce).

Oncomine and TCGA

Using Oncomine analysis, MSI1 expression was analyzed in the Kaiser colon database. The database includes full transcriptome profiles of 105 samples: Control (5); Cecum Adenocarcinoma (17); Colon Adenocarcinoma (41); Colon Mucinous Adenocarcinoma (13); Colon Signet Ring Cell Adenocarcinoma (2); Colon Small Cell Carcinoma (2); Rectal Adenocarinoma (8); Rectal Mucinous Adenocarcinoma (4); Rectal Signet Ring Cell Adenocarcinoma (1); Rectosigmoid Adenocarcinoma (10); Rectosigmoid Mucinous Adenocarcinoma (2).(Rhodes et al., 2007) For TCGA analysis, fold changes for MSI1 in matched tumor/control RNA-Seq sample pairs from TCGA COAD were calculated (total of 26 patients.) Distribution of MSI1 fold changes in tumor/control pairs for 26 individuals plotted are in red (intra-individual comparison). Distribution of MSI1 fold changes between control/control comparisons for 26 distinct individuals plotted in grey (inter-individual comparison).

PTEN Immunoprecipitation and Activity Assay

Cells (293 & RKO) from a 100 mm culture dish at 70-80% were lysed with 0.5 mL of ice cold IP Lysis Buffer (25mM Tris pH 8.0, 150 mM NaCl, 1% NP-40, 1mM EDTA, 5% Glycerol). 400 µL of the cell lysate was Transferred to a fresh, cold, 1.5 mL centrifuge tube. 8 µL of the anti-PTEN antibody (Cell Signaling, #9188) was added to the lysate followed by overnight incubation at 4°C with agitation. 60 µL of the Protein A Dynabeads was added to the mixture and incubated 2-3 hours at 4°C. The bead complex was washed and resuspended in 30 µL of PTEN Reaction buffer. Proceed immediately with the PTEN reactions by adding 30 µL of the 16 µM PI(3,4,5)P3 Substrate to the bead complex. The ELISA was performed following manufacturer's protocol (Echelon, K-4700).

PIP3 Flow Cytometry

Colorectal cancer cell lines were cultured in DMEM+ 10% FBS and transfected with pSico vector to knockdown Msi1 and Msi2 using Fugene HD (Promega) according to user manual.

EGFP is expressed from pSico as a marker to select for transfected cells. Transfected cells were harvested by trypsinization 72 hours post-transfection, washed and resuspended in PBS containing 1 uL/ml of fixable viability dye eFluor 450(Affymetrix ebioscience). Cells were incubated on ice for 30 minutes and were washed two times with PBS. Then, cells were fixed and permeabilized using Cytofix/ Cytoperm solution (BD PharMingen), stained with FITC-anti-GFP (Abcam) and biotinylated anti-PIP3 (Echelon inc.) for 30 min on ice and washed twice. They were incubated with Streptavidin-Allophycocyanin (APC) (biolegend) for 30 min on ice and washed twice. Flow cytometry was performed on LSRFoirtessa and Flowjo software was used for data analysis.

qRT-PCR

Human colorectal cancer cell lines were grown to 60-80% confluence followed by RNA extraction with TRIzol. Normal human colon samples were obtained from the Cooperative Human Tissue Network (CHTN) in cooperation with the University of Pennsylvania Center for Molecular Studies in Digestive and Liver Diseases Molecular Biology and Gene Expression Core. RNA from human colon samples and intestinal organoids was isolated with TRIzol.

1ug total RNA was used for reverse transcription in 20ul total volume with High-Capacity cDNA Reverse Transcription Kit (Life Technologies, Cat. No. 4368813). For qRT-PCR, 1ul cDNA product was used for each reaction. Primer sequences used for human MSI1 and MSI2 are as follows: *MSI1#1* Forward: 5'-GCCATGCTGATGTTCGACAA, Reverse: 5'-CTACGATGTCCTCGCTCTCAA. *MSI1#2* Forward: 5'-AGGACTCAGTTGGCAGACC, Reverse: 5'-GCATCACCAGACACTCTTTCAC. *MSI2#1* Forward: 5'-GCGATGCTGATGTTCGACAA, Reverse: 5'-TCTCCACAACGTCTTCATTCTCA. *MSI2#2* Forward: 5'-ATTTGCTCCTAGCTATGGCTACC, Reverse: 5'-CGCTGCCACTGGTCCATA

Xenograft Assays

6-week-old female nude mice were obtained from the Stem Cell and Xenograft Core at UPENN. Stably infected colorectal cancer cells were trypsinized and suspended in phosphate-buffered saline (PBS). A total volume of 0.2 ml containing 2-5 X 10^6 cells and 25% volume MatriGEL was injected subcutaneously into the mouse flank. Tumor size was

measured using a Vernier caliper. Tumor volumes were calculated using the formula V=1⁄2 (LxW^2), where L is length (longest dimension) and W is width (shortest dimension) of the tumor. Moribund animals were euthanized according to the protocols of the University of Pennsylvania. Tumor growth rates in the xenograft experiment were evaluated by fitting a linear mixed effects model on the log_{10}-transformed tumor volume with days, experiment indicator (Msi shRNA versus control shRNA), and interaction between days and experiment included as independent variables.nat

Supplemental References

Kinzler, K.W., Nilbert, M.C., Su, L.K., Vogelstein, B., Bryan, T.M., Levy, D.B., Smith, K.J., Preisinger, A.C., Hedge, P., McKechnie, D.*, et al.* (1991). Identification of FAP locus genes from chromosome 5q21. Science *253*, 661-665.

Levin, T.G., Powell, A.E., Davies, P.S., Silk, A.D., Dismuke, A.D., Anderson, E.C., Swain, J.R., and Wong, M.H. (2010). Characterization of the intestinal cancer stem cell marker CD166 in the human and mouse gastrointestinal tract. Gastroenterology *139*, 2072-2082 e2075.

Li, D., Peng, X., Yan, D., Tang, H., Huang, F., Yang, Y., and Peng, Z. (2011). Msi-1 is a predictor of survival and a novel therapeutic target in colon cancer. Ann Surg Oncol *18*, 2074-2083.

Li, N., Yousefi, M., Nakauka-Ddamba, A., Jain, R., Tobias, J., Epstein, J.A., Jensen, S.T., and Lengner, C.J. (2014). Single-cell analysis of proxy reporter allele-marked epithelial cells establishes intestinal stem cell hierarchy. Stem cell reports *3*, 876-891.

Madison, B.B., Liu, Q., Zhong, X., Hahn, C.M., Lin, N., Emmett, M.J., Stanger, B.Z., Lee, J.S., and Rustgi, A.K. (2013). LIN28B promotes growth and tumorigenesis of the intestinal epithelium via Let-7. Genes Dev *27*, 2233-2245.

Marsh, V., Winton, D.J., Williams, G.T., Dubois, N., Trumpp, A., Sansom, O.J., and Clarke, A.R. (2008). Epithelial Pten is dispensable for intestinal homeostasis but suppresses adenoma development and progression after Apc mutation. Nat Genet *40*, 1436-1444.

Miyoshi, Y., Nagase, H., Ando, H., Horii, A., Ichii, S., Nakatsuru, S., Aoki, T., Miki, Y., Mori, T., and Nakamura, Y. (1992). Somatic mutations of the APC gene in colorectal tumors: mutation cluster region in the APC gene. Hum Mol Genet *1*, 229-233.

Nagase, H., Miyoshi, Y., Horii, A., Aoki, T., Petersen, G.M., Vogelstein, B., Maher, E., Ogawa, M., Maruyama, M., Utsunomiya, J.*, et al.* (1992). Screening for germ-line mutations in familial adenomatous polyposis patients: 61 new patients and a summary of 150 unrelated patients. Hum Mutat *1*, 467-473.

Naguib, A., Cooke, J.C., Happerfield, L., Kerr, L., Gay, L.J., Luben, R.N., Ball, R.Y., Mitrou, P.N., McTaggart, A., and Arends, M.J. (2011). Alterations in PTEN and PIK3CA in colorectal cancers in the EPIC Norfolk study: associations with clinicopathological and dietary factors. BMC cancer *11*, 123.

Nakamura, M., Okano, H., Blendy, J.A., and Montell, C. (1994). Musashi, a neural RNA-binding protein required for Drosophila adult external sensory organ development. Neuron *13*, 67-81.

Okabe, M., Imai, T., Kurusu, M., Hiromi, Y., and Okano, H. (2001). Translational repression determines a neuronal potential in Drosophila asymmetric cell division. Nature *411*, 94-98.

Okano, H., Imai, T., and Okabe, M. (2002). Musashi: a translational regulator of cell fate. J Cell Sci *115*, 1355-1359.

Park, S.M., Deering, R.P., Lu, Y., Tivnan, P., Lianoglou, S., Al-Shahrour, F., Ebert, B.L., Hacohen, N., Leslie, C., Daley, G.Q.*, et al.* (2014). Musashi-2 controls cell fate, lineage bias, and TGF-beta signaling in HSCs. The Journal of experimental medicine *211*, 71-87.

Park, S.M., Gonen, M., Vu, L., Minuesa, G., Tivnan, P., Barlowe, T.S., Taggart, J., Lu, Y., Deering, R.P., Hacohen, N.*, et al.* (2015). Musashi2 sustains the mixed-lineage leukemia-driven stem cell regulatory program. The Journal of clinical investigation *125*, 1286-1298.

Potten, C.S., Booth, C., Tudor, G.L., Booth, D., Brady, G., Hurley, P., Ashton, G., Clarke, R., Sakakibara, S., and Okano, H. (2003). Identification of a putative intestinal stem cell and early lineage marker; musashi-1. Differentiation *71*, 28-41.

Powell, A.E., Wang, Y., Li, Y., Poulin, E.J., Means, A.L., Washington, M.K., Higginbotham, J.N., Juchheim, A., Prasad, N., Levy, S.E.*, et al.* (2012). The pan-ErbB negative regulator Lrig1 is an intestinal stem cell marker that functions as a tumor suppressor. Cell *149*, 146-158.

Rezza, A., Skah, S., Roche, C., Nadjar, J., Samarut, J., and Plateroti, M. (2010). The overexpression of the putative gut stem cell marker Musashi-1 induces tumorigenesis through Wnt and Notch activation. J Cell Sci *123*, 3256-3265.

Sakakibara, S., Nakamura, Y., Yoshida, T., Shibata, S., Koike, M., Takano, H., Ueda, S., Uchiyama, Y., Noda, T., and Okano, H. (2002). RNA-binding protein Musashi family: roles for CNS stem cells and a subpopulation of ependymal cells revealed by targeted disruption and antisense ablation. Proceedings of the National Academy of Sciences of the United States of America *99*, 15194-15199.

Sanchez-Diaz, P.C., Burton, T.L., Burns, S.C., Hung, J.Y., and Penalva, L.O. (2008). Musashi1 modulates cell proliferation genes in the medulloblastoma cell line Daoy. BMC cancer *8*, 280.

Sansom, O.J., Reed, K.R., Hayes, A.J., Ireland, H., Brinkmann, H., Newton, I.P., Batlle, E., Simon-Assmann, P., Clevers, H., Nathke, I.S.*, et al.* (2004). Loss of Apc in vivo immediately perturbs Wnt signaling, differentiation, and migration. Genes Dev *18*, 1385-1390.

Spears, E., and Neufeld, K.L. (2011). Novel double-negative feedback loop between adenomatous polyposis coli and Musashi1 in colon epithelia. The Journal of biological chemistry *286*, 4946-4950.

Subramanian, A., Tamayo, P., Mootha, V.K., Mukherjee, S., Ebert, B.L., Gillette, M.A., Paulovich, A., Pomeroy, S.L., Golub, T.R., Lander, E.S.*, et al.* (2005). Gene set enrichment analysis: a knowledge-based approach for interpreting genome-wide expression profiles. Proceedings of the National Academy of Sciences of the United States of America *102*, 15545-15550.

Sugiyama-Nakagiri, Y., Akiyama, M., Shibata, S., Okano, H., and Shimizu, H. (2006). Expression of RNA-binding protein Musashi in hair follicle development and hair cycle progression. The American journal of pathology *168*, 80-92.

Sureban, S.M., May, R., George, R.J., Dieckgraefe, B.K., McLeod, H.L., Ramalingam, S., Bishnupuri, K.S., Natarajan, G., Anant, S., and Houchen, C.W. (2008). Knockdown of RNA binding protein musashi-1 leads to tumor regression in vivo. Gastroenterology *134*, 1448-1458.

Sutherland, J.M., Fraser, B.A., Sobinoff, A.P., Pye, V.J., Davidson, T.L., Siddall, N.A., Koopman, P., Hime, G.R., and McLaughlin, E.A. (2014). Developmental expression of Musashi-1 and Musashi-2 RNA-binding proteins during spermatogenesis: analysis of the deleterious effects of dysregulated expression. Biology of reproduction *90*, 92.

Uren, P.J., Vo, D.T., de Araujo, P.R., Potschke, R., Burns, S.C., Bahrami-Samani, E., Qiao, M., de Sousa Abreu, R., Nakaya, H.I., Correa, B.R.*, et al.* (2015). RNA-Binding Protein Musashi1 Is a Central Regulator of Adhesion Pathways in Glioblastoma. Molecular and cellular biology *35*, 2965-2978.

van Hogezand, R.A., Eichhorn, R.F., Choudry, A., Veenendaal, R.A., and Lamers, C.B. (2002). Malignancies in inflammatory bowel disease: fact or fiction? Scandinavian journal of gastroenterology Supplement, 48-53.

Vo, D.T., Subramaniam, D., Remke, M., Burton, T.L., Uren, P.J., Gelfond, J.A., de Sousa Abreu, R., Burns, S.C., Qiao, M., Suresh, U.*, et al.* (2012). The RNA-binding protein Musashi1 affects medulloblastoma growth via a network of cancer-related genes and is an indicator of poor prognosis. The American journal of pathology *181*, 1762-1772.

Wang, S., Li, N., Yousefi, M., Nakauka-Ddamba, A., Li, F., Parada, K., Rao, S., Minuesa, G., Katz, Y., Gregory, B.D.*, et al.* (2015). Transformation of the intestinal epithelium by the MSI2 RNA-binding protein. Nature communications *6*, 6517.

Wang, X.Y., Yin, Y., Yuan, H., Sakamaki, T., Okano, H., and Glazer, R.I. (2008). Musashi1 modulates mammary progenitor cell expansion through proliferin-mediated activation of the Wnt and Notch pathways. Molecular and cellular biology *28*, 3589-3599.

Wasan, H.S., Park, H.S., Liu, K.C., Mandir, N.K., Winnett, A., Sasieni, P., Bodmer, W.F., Goodlad, R.A., and Wright, N.A. (1998). APC in the regulation of intestinal crypt fission. J Pathol *185*, 246-255.